Supplementary Information

^{7}Li NMR Chemical Shift Imaging to Detect Microstructural Growth of Lithium in All Solid-State Batteries

Lauren E. Marbella,[a‡] Stefanie Zekoll,[b‡] Jitti Kasemchainan,[b] Steffen P. Emge,[a] Peter G. Bruce,[b] Clare P. Grey*[a]

[a]Department of Chemistry, University of Cambridge, Lensfield Road, Cambridge CB2 1EW, United Kingdom
[b]Department of Materials, University of Oxford, Parks Road, Oxford OX1 3PH, UK

Table of Contents

X-ray diffraction.

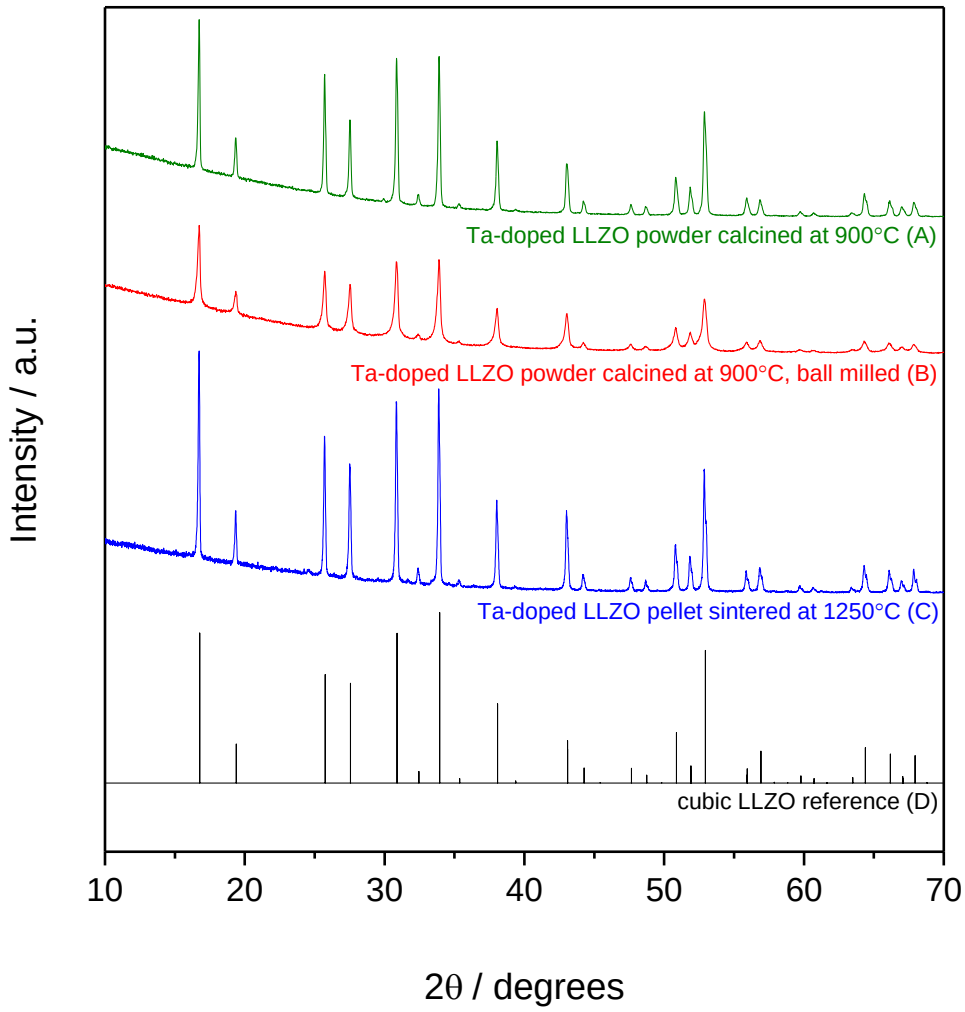

Figure S1. XRD patterns of (A) Ta-doped LLZO powder calcined at 900 °C (green), (B) Ta-doped LLZO powder calcined at 900 °C after ball milling (red), (C) Ta-doped LLZO pellet sintered at 1250 °C (blue), and (D) cubic LLZO reference (black).

Electrochemical measurements.

The voltage profile of the short-circuited Li-LLZTO-Li cell discussed in Figure 1b is shown below (Figure S2). The cell was first cycled at a current density of 0.2 $mA \cdot cm^{-2}$ up to a capacity of

1.0 $mAh \cdot cm^{-2}$ for 3 cycles, then at a current density of 0.5 $mA \cdot cm^{-2}$ up to a capacity of 1.0 $mAh \cdot cm^{-2}$ for 3 cycles, followed by 3 cycles at a current density of 1.0 $mA \cdot cm^{-2}$ up to a capacity of 1.0 $mAh \cdot cm^{-2}$ and finally, again, at a current density of 0.5 $mA \cdot cm^{-2}$ for one discharge until short-circuiting occurred. Due to the increased thickness of this pellet compared to all other pellets used (3.95 mm), the cell lasted for several cycles above 0.5 $mA \cdot cm^{-2}$. Nevertheless, the voltage curves at 1.0 $mA \cdot cm^{-2}$ do show significant fluctuations in cell voltage, which suggest extensive dendrite growth is occurring at 1.0 $mA \cdot cm^{-2}$, but that these dendrites have not yet fully reached the other electrode to cause a short circuit due to the increased thickness of the electrolyte. However, applying a current density of 0.5 $mA \cdot cm^{-2}$ after cycling at 1.0 $mA \cdot cm^{-2}$ instantaneously led to short circuit of the cell.

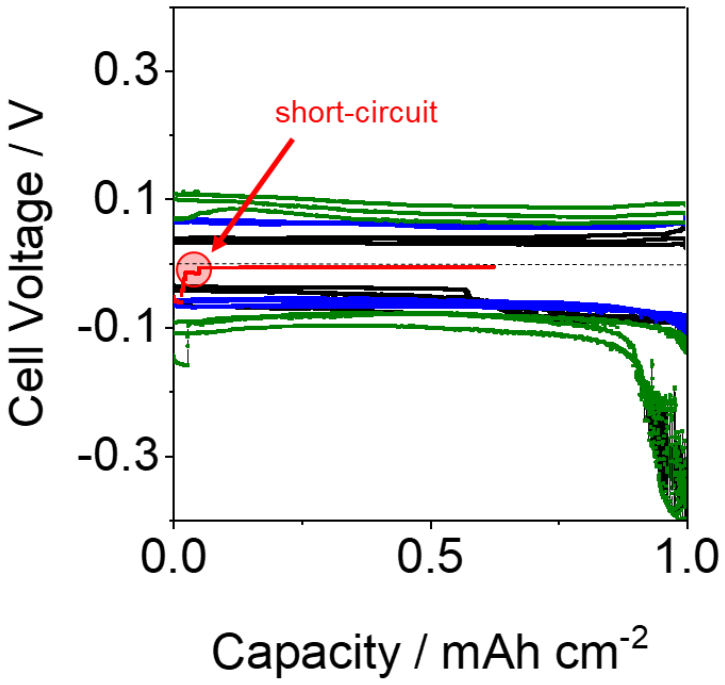

Figure S2. Voltage profile of the short circuited Li-LLZTO-Li symmetrical cell discussed in Figure 1b of the main text cycled at 0.2 $mA \cdot cm^{-2}$ up to a capacity of 1.0 $mAh \cdot cm^{-2}$ for 3 cycles (black), followed by 0.5 $mA \cdot cm^{-2}$ up to a capacity of 1.0 $mAh \cdot cm^{-2}$ for 3 cycles (blue), 1.0 $mA \cdot cm^{-2}$ up to a capacity of 1.0 $mAh \cdot cm^{-2}$ for 3 cycles (green) and finally at 0.5 $mA \cdot cm^{-2}$ for one discharge only until short circuit (red).

The relationship between LLZTO thickness and the time the cell takes to short circuit at 0.5 $mA \cdot cm^{-2}$ is shown in Figure S3. The thicker the LLZTO pellet, the longer the cell can be discharged at a current density of 0.5 $mA \cdot cm^{-2}$ before short circuit.

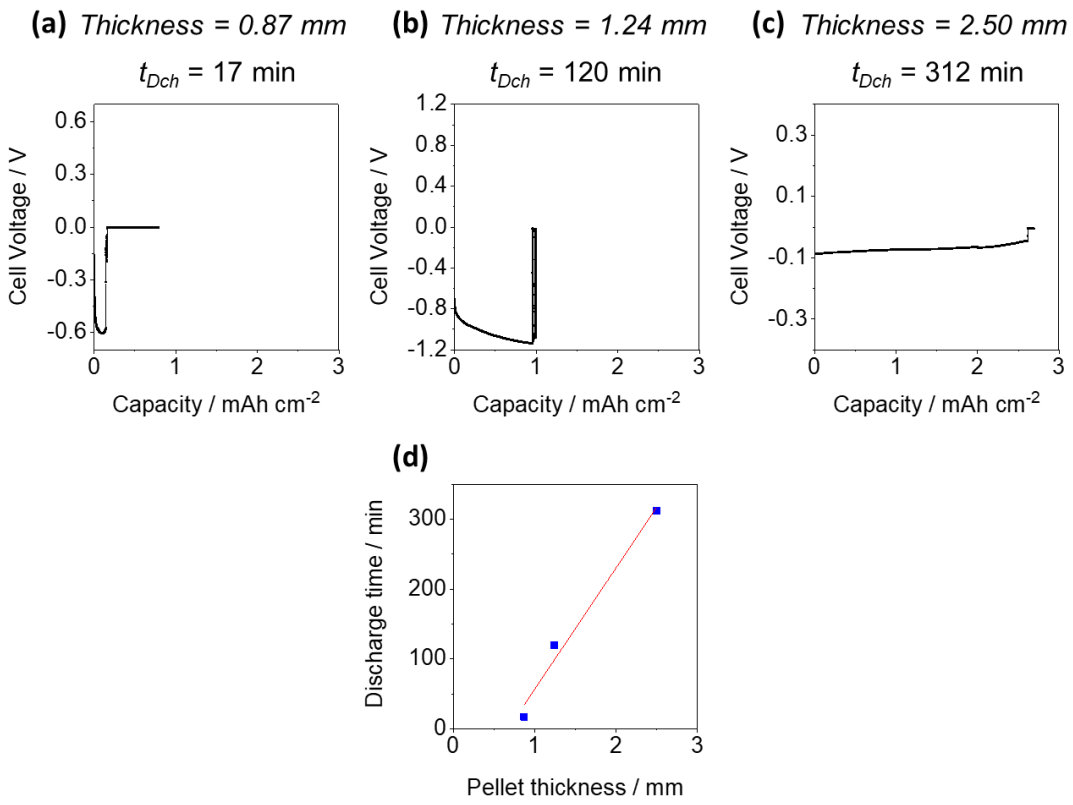

Figure S3. Voltage profiles of short circuit Li-LLZTO-Li cells with cell thicknesses of 0.87 mm (a), 1.24 mm (b), and 2.50 mm (c) discharged at 0.5 mA·cm^{-2} until short circuit. The linear relationship between pellet thickness and discharge time until short circuit is shown in (d).

Table S1. Ionic conductivity and density of the Li-LLZTO-Li pellets shown in Figures 3 and 5 of the main text.

Figure	Pellet Name	Ionic Conductivity (S cm^{-1})	Density (g cm^{-3})	% density (theoretical density ~5.31 g cm^{-3})
Figure 1b	LLZO-211217-6	/	4.51	85
Figure 1c	LLZO-290317-1	1.2×10^{-3}	4.70	89
Figure 3a	LLZO-211217-6	/	4.51	85
Figure 3b	LLZO-201117-3	8.7×10^{-4}	4.80	90
Figure 3c	LLZO-201117-1	1.4×10^{-3}	4.76	90
Figure 3d	LLZO-211217-5	6.1×10^{-4}	4.80	90
Figure 3e	LLZO-211217-2b	5.5×10^{-4}	4.65	88
Figure 3f	LLZO-201217-1c	8.6×10^{-4}	4.76	90
Figure 3g	LLZO-211217-3a	1.2×10^{-3}	4.62	87
Figure 5a	LLZO-090318-1	1.2×10^{-3}	4.56	86
Figure 5b	LLZO-090318-2	1.4×10^{-3}	4.62	87

Table S2. EIS analysis of the Li-LLZTO-Li cells in Figure 3 of the main text at various time points during their cycling, where the resistances, R1–R3 (bulk, grain boundary and interface, respectively) and capacitances C1–C3, for the three constant phase elements are defined in Figure S4.

Figure 3b		
Cycle time (min)	0	30
R1 (Ω·cm)	849	778
C1 (F/cm)	2.E-09	1.E-08
R2 (Ω·cm)	290	226
C2 (F/cm)	6.E-08	6.E-08
R3 (Ω·cm2)	27	34
C3 (F/cm2)	4.E-02	1.E-01
Rtotal (Ω·cm)	1249	1138

Figure 3c		
Cycle time (min)	0	120
R1 (Ω·cm)	434	483
C1 (F/cm)	1.E-09	1.E-09
R2 (Ω·cm)	253	144
C2 (F/cm)	1.E-08	3.E-08
R3 (Ω·cm2)	14	47
C3 (F/cm2)	9.E-03	2.E-01
Rtotal (Ω·cm)	743	813

Figure 3d			
Cycle time (min)	0	120	240
R1 (Ω·cm)	1002	525	666
C1 (F/cm)	7.E-10	7.E-10	7.E-10
R2 (Ω·cm)	600	344	184
C2 (F/cm)	1.E-08	3.E-08	8.E-09
R3 (Ω·cm2)	50	69	65
C3 (F/cm2)	9.E-04	1.E-02	9.E-01
Rtotal (Ω·cm)	1829	1179	1140

Figure 3e				
Cycle time (min)	0	120	240	293
R1 (Ω·cm)	1054	645	669	EIS not recorded
C1 (F/cm)	9.E-10	9.E-10	9.E-10	
R2 (Ω·cm)	673	429	354	
C2 (F/cm)	2.E-08	3.E-08	5.E-09	
R3 (Ω·cm2)	41	43	48	
C3 (F/cm2)	2.E-04	2.E-01	8.E-04	
Rtotal (Ω·cm)	1883	1236	1203	

Figure 3f					
Cycle time (min)	0	120	240	360	480
R1 (Ω·cm)	616	476	483	285	439
C1 (F/cm)	9.E-10	8.E-10	9.E-10	1.E-09	9.E-10
R2 (Ω·cm)	536	136	293	192	264
C2 (F/cm)	1.E-08	6.E-08	6.E-09	4.E-09	6.E-09
R3 (Ω·cm2)	39	23	**129**	63	**188**
C3 (F/cm2)	2.E-03	2.E+01	7.E+00	5.E+00	1.E+00
Rtotal (Ω·cm)	1314	705	1305	734	1472

Figure 3g							
Cycle time (min)	0	120	240	360	480	600	720
R1 (Ω·cm)	505	406	358	337	270	165	no data fitting possible, cell short-circuited
C1 (F/cm)	1.E-09	1.E-09	1.E-09	9.E-10	1.E-09	7.E-10	
R2 (Ω·cm)	357	160	138	48	150	2	
C2 (F/cm)	6.E-09	8.E-09	5.E-09	3.E-08	4.E-09	5.E-05	
R3 (Ω·cm2)	12	11	54	62	**272**	8	
C3 (F/cm2)	5.E-03	9.E-03	7.E-01	1.E+02	2.E+03	1.E+00	
Rtotal (Ω·cm)	905	608	699	618	1436	196	

An equivalent circuit composed of a series of three resistors and constant-phase elements in parallel to account for the bulk (R1), grain boundary (R2), and interface (R3) resistances present within the cell was used to fit the data (see schematic below) The capacitance values for each resistance are labeled as C1, C2, and C3, respectively. The total resistance of the cell (Rtotal) for each time point is also calculated.

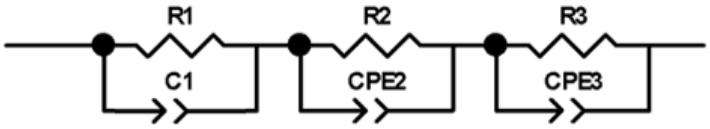

Figure S4. Schematic of the equivalent circuit composed of a series of three resistors and constant-phase elements in parallel to account for the bulk (R1), grain boundary (R2) and interface (R3) resistances present within the cell was used to fit EIS data.

Significant increases in the interface resistance (R3) are labelled in red in Table S2. It should be noted that low frequency behaviors in Nyquist plots such as the interface resistance are much harder to fit than the bulk and grain boundary resistances, at least for our data, and therefore should not be regarded as absolute. Additionally, from our EIS analysis and voltage profiles of the cells in Figure 3, it is only just before cell failure that major changes in the EIS or cell voltage are observed. No information on the initial growth of microstructural Li can be extracted. Hence, ^{7}Li CSI could, in the long run, be more useful in providing a new dimension to study dendrite growth and cell failure, especially at visualizing Li metal growth at the very early stages of cycling.

All Nyquist plots obtained during cycling of cells in Figure 3f and 3g of the main text are shown in Figure S5. These plots show alternating higher and lower total impedances depending

on the current direction for the cell in Figure 3f, and a clear decrease in total impedance for the cell in Figure 3g as current is passed. Both Nyquist plots after 600 minutes and 720 minutes for the cell in Figure 3g suggest that a short-circuit has occurred.

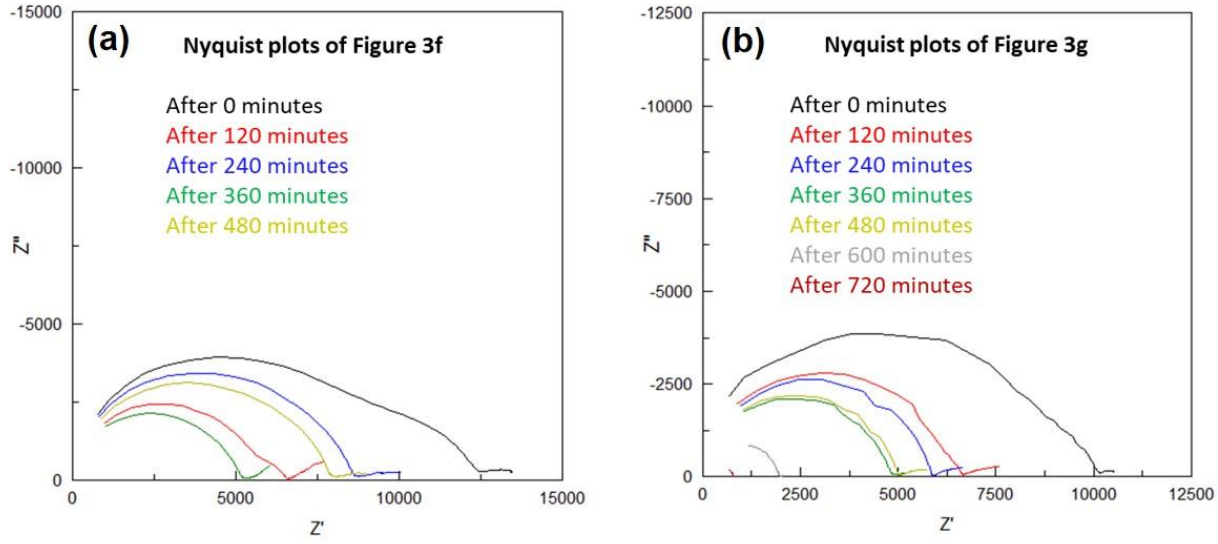

Figure S5. Nyquist plots at different stages of cycling for the Li-LLZTO-Li cells shown in the main text Figure 3f (a) and 3g (b).

Table S3. EIS measurements for the Li-LLZTO-Li cell shown in Figure 4.

	From EIS measurements		From voltage curves
	Total Resistance (Ohm cm)	σ (S cm^{-1})	Cell Voltage at the end of each cycle (mV)
After cell-assembly	868	1.2×10^{-3}	/
After 1st cycle	852	1.2×10^{-3}	59.9
After 2nd cycle	805	1.2×10^{-3}	57.1
After 3rd cycle	790	1.3×10^{-3}	55.9
After 5th cycle	620	1.6×10^{-3}	48.3
After 10th cycle	542	1.8×10^{-3}	42.0
After 20th cycle	488	2.0×10^{-3}	37.6
After 30th cycle	491	2.0×10^{-3}	38.2
After 40th cycle	523	1.9×10^{-3}	39.2

^{7}Li chemical shift imaging.

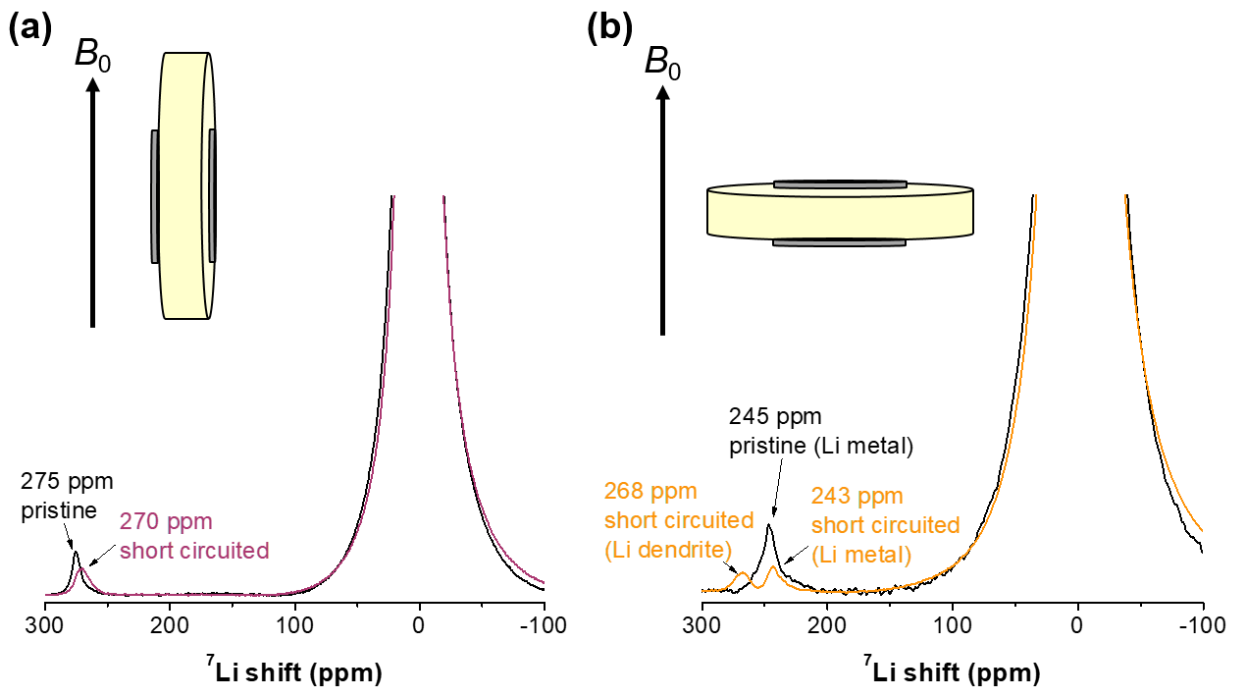

Figure S6. ^{7}Li NMR of pristine (black) and short circuited (purple in (a) and orange in (b)) Li-LLZTO-Li symmetrical cells with the electrodes oriented (a) parallel and (b) perpendicular to B_0.

Figure S6 illustrates the effect of orientation on the shift of the Li metal signal. If the electrodes were oriented parallel to B_0, the resolution between the dendrites and the Li metal electrodes was significantly worse than the perpendicular orientation (Figure S6). For each sample, single pulse ^{7}Li NMR spectra were collected with a recycle delay of 1 s and 2048 scans. Typical 90° radiofrequency (rf) pulses were approximately 12 μs for ^{7}Li. ^{7}Li CSI were recorded using a single phase encoded spatial dimension.[1] Typical experiment times for ^{7}Li CSI ranged from *ca.* 7–15 h. Suitable signal could be achieved within 1–2 h for most samples, but longer experiments were run to collect additional signal from low intensity Li dendrite species (and to ensure their absence at low cycling times).

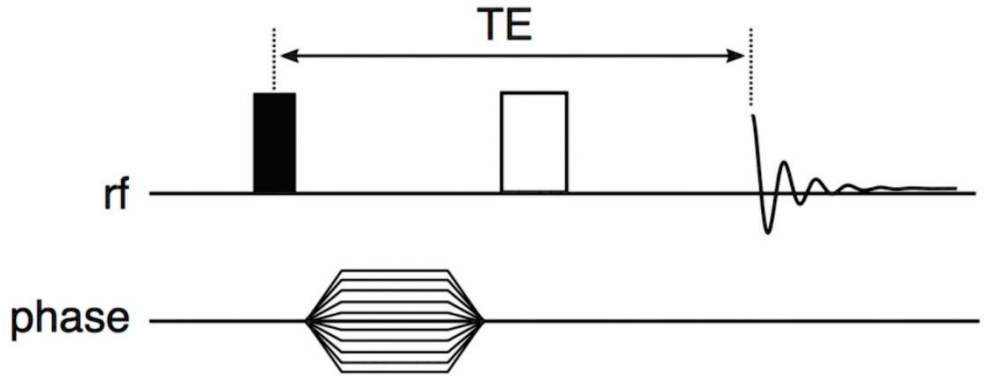

Figure S7. Pulse sequence used for ^{7}Li chemical shift imaging experiments with a single phase-encoded spatial dimension. The black rectangle represents 90° rf pulses, whereas the white rectangle represents a 180° rf pulse. Figure reproduced with permission from ref 1. Copyright 2015 American Chemical Society.

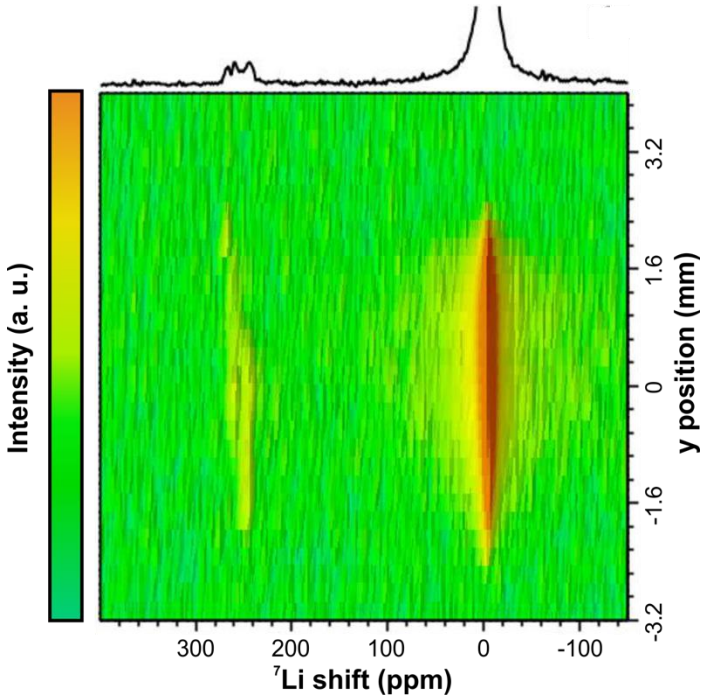

Figure S8. Li-LLZTO-Li symmetrical cell cycled at a current density of 0.2 mA·cm^{-2} to 1.0 mA·cm^{-2} until short-circuit (same cell as Figure 1c). ^{7}Li MRI was performed in the y dimension to show lateral information.

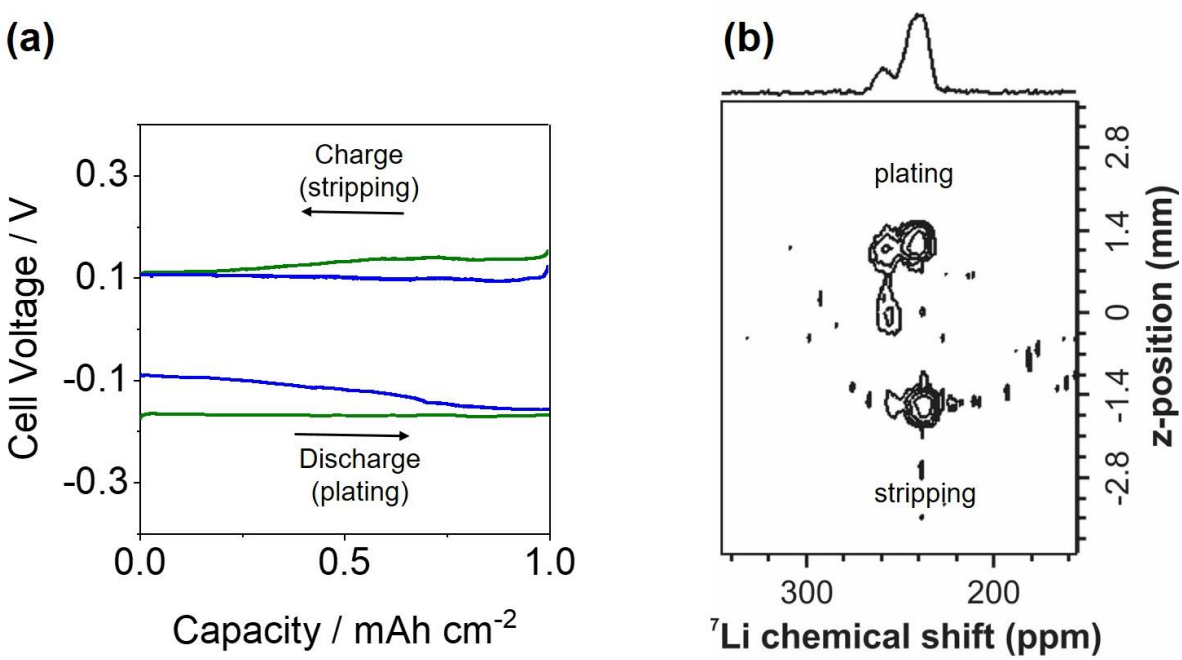

Figure S9. (a) Galvanostatic cycling at 0.5 mA/cm^2 for up to 2 h per charge/discharge with the first cycle shown in green and the second cycle shown in blue. The cell was stopped at t_{cyc} = 480 min and analyzed with (b) ^{7}Li CSI.

References

1. Chang, H. J.; Ilott, A. J.; Trease, N. M.; Mohammadi, M.; Jerschow, A.; Grey, C. P., Correlating Microstructural Lithium Metal Growth with Electrolyte Salt Depletion in Lithium Batteries Using ^{7}Li MRI. *J. Am. Chem. Soc.* **2015,** *137,* 15209-15216.